ACS APPLIED MATERIALS & INTERFACES

Research Article

www.acsami.org

Facile Synthesis of $Na_{0.33}V_2O_5$ Nanosheet-Graphene Hybrids as Ultrahigh Performance Cathode Materials for Lithium Ion Batteries

Yakun Lu,[†,‡] Jun Wu,[†,‡] Jun Liu,[*,†,‡] Ming Lei,[§] Shasha Tang,[†,‡] Peijie Lu,[†,‡] Linyu Yang,[†,‡] Haoran Yang,[†,‡] and Qian Yang[†,‡]

[†]School of Materials Science and Engineering and [‡]Education Ministry Key Laboratory of Non-ferrous Materials Science and Engineering, Central South University, Changsha, Hunan 410083, People's Republic of China

[§]State Key Laboratory of Information Photonics and Optical Communications, Beijing University of Posts and Telecommunications, Beijing 100876, People's Republic of China

Supporting Information

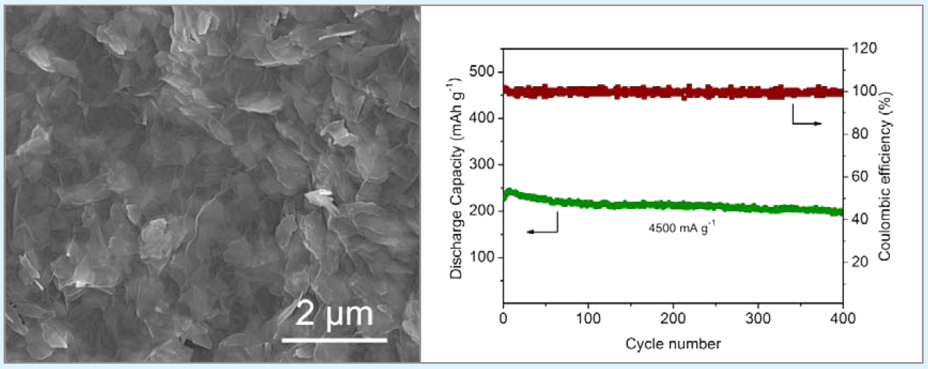

ABSTRACT: $Na_{0.33}V_2O_5$ nanosheet-graphene hybrids were successfully fabricated for the first time via a two-step route involving a novel hydrothermal method and a freeze-drying technique. Uniform $Na_{0.33}V_2O_5$ nanosheets with a thickness of about 30 nm are well-dispersed between graphene layers. The special sandwich-like nanostructures endow the hybrids with high discharge capacity, good cycling stability, and superior rate performance as cathodes for lithium storage. Desirable discharge capacities of 313, 232, 159, and 108 mA·h·g^{-1} can be delivered at 0.3, 3, 6, and 9 A·g^{-1}, respectively. Moreover, the $Na_{0.33}V_2O_5$-graphene hybrids can maintain a high discharge capacity of 199 mA·h·g^{-1} after 400 cycles even at an extremely high current density of 4.5 A·g^{-1}, with an average fading rate of 0.03% per cycle.

KEYWORDS: *lithium ion batteries, $Na_{0.33}V_2O_5$ nanosheet-graphene hybrids, facile synthesis, sandwich-like nanostructures, high-rate performance*

INTRODUCTION

Rechargeable lithium ion batteries (LIBs) have been widely used in portable electronics and become the prime candidate to power electric vehicles, since they possess attractive characteristics, such as high energy density, long lifespan, and environmental friendliness.[1] However, the unsatisfactory specific capacities of current commercial cathodes block the further application of LIBs. For instance, $LiCoO_2$, $LiMn_2O_4$, and $LiFePO_4$, the most commonly used cathodes, deliver low reversible capacities (<180 mA·h·g^{-1}).[2] Therefore, cathode materials with higher energy and power densities must be developed to meet the ever-increasing demand for high-performance LIBs.

Over the past decades, vanadium oxides and vanadates have been extensively studied as cathode materials for LIBs due to their high capacities, low cost, and abundant resources.[3−11] Among those compounds, vanadium pentoxide (V_2O_5) with layered structure exhibits a high theoretical capacity of 442 mA·h·g^{-1} when three lithium ions are intercalated, thus becoming one of the most promising candidates. But bulk V_2O_5 suffers from intrinsic low lithium ion diffusion coefficient (~10^{-12} cm^2·s^{-1}), poor electronic conductivity (10^{-2}−10^{-3} S·cm^{-1}), and structural instability upon deep charge and discharge.[12,13] One of possible strategies is introducing second metal cations (Na^+, Ag^+, and Li^+, et al.) into the V_2O_5 interlayer, since those ions can act as "pillars" to improve structural stability and provide a fast diffusion path.[14] Among them, β-$Na_{0.33}V_2O_5$ with a rigid three-dimensional (3D) framework has drawn much attention.[15−17]

As shown in Figure 1, there are three crystallographically different vanadium sites in β-$Na_{0.33}V_2O_5$, namely, V(1), V(2), and V(3).[18] The edge-sharing $V(1)O_6$ octahedra and corner-sharing $V(2)O_6$ octahedra form zigzag chains and double chains along the b axis, respectively, which are further linked by

Received: June 2, 2015
Accepted: July 21, 2015
Published: July 21, 2015

DOI: 10.1021/acsami.5b04827
ACS Appl. Mater. Interfaces 2015, 7, 17433−17440

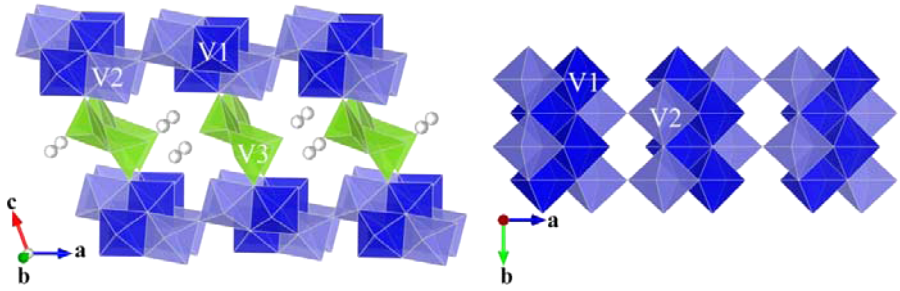

Figure 1. Crystal structure of β-$Na_{0.33}V_2O_5$.

oxygen atoms and constitute $[V_4O_{11}]_n$ layers along the (001) plane. The zigzag chains composed of edge-sharing $V(3)O_5$ pyramids connect the $[V_4O_{11}]_n$ layers, thus forming the 3D tunnelled structure. Baddour-Hadjean et al. studied the structural behaviors of β-$Na_{0.33}V_2O_5$ during discharge in the potential range of 2.2−3.8 V.[15] They found that the overall structural changes of β-$Na_{0.33}V_2O_5$ were negligible, since the 3D structure could diminish the structural stress induced by lithium insertion. Highly ordered single crystalline NaV_6O_{15} nanorods were fabricated and exhibited specific discharge capacities as high as 328 and 300 mA·h·g^{-1} at current densities of 20 and 50 mA·g^{-1}.[9] Recently, Liang et al. prepared mesoporous β-$Na_{0.33}V_2O_5$ exhibiting specific discharge capacities of 339 and 226 mA·h·g^{-1} at 20 and 300 mA·g^{-1}, respectively.[16] Despite these structural advantages and some nanostructured β-$Na_{0.33}V_2O_5$ being synthesized, the practical application of this material remains a challenge. β-$Na_{0.33}V_2O_5$ requires further modifications to overcome certain limitations, such as large resistance polarization and poor rate capability. Therefore, reducing the particle size and hybridization with electronically conductive materials are necessary for this material.

Two-dimensional (2D) nanosheets, especially those with lateral dimension of sub-micrometers to micrometers and thickness less than several tens of nanometers, can be considered as a new class of inorganic macromolecules with high surface areas and unique electronic properties that are important for sensing,[19] catalysis,[20] and energy storage.[21−25] In particular, 2D nanosheets are ideal structures for fast lithium storage, since they can provide a short lithium ion diffusion path, a two-dimensional carrier pathway, and a high active surface area compared with bulk materials.[26] Recently, a lot of inorganic materials with nanosheet structures have been synthesized, such as BN,[27] MoS_2,[28] MnO_2,[29] $Ni(OH)_2$,[30] and $Co(OH)_2$.[31] Unfortunately, in most cases, materials with nanosheet morphology essentially have layered crystal structures. This is a major obstacle for exploiting other materials, especially those without layered crystal structures. Some efforts have been devoted to synthesizing nonlayered-structure ternary materials with thin nanosheet structures, such as $Li_4Ti_5O_{12}$[32] and Li_3VO_4 nanosheets.[33] Nevertheless, it remains challenging to fabricate monoclinic β-$Na_{0.33}V_2O_5$ with uniform and thin nanosheet morphology due to its nonlayered crystal structure.

On the other hand, hybridization with carbon materials is a practical and effective method to enhance electronic conductivity of electrodes. Nanocomposites modified by carbon materials (such as graphene,[33−37] CNTs,[38,39] and carbon[40]) are intensively studied for LIBs. Specifically, graphene as a two-dimensional carbon material, exhibiting superior electrical conductivity, large surface area, and structural flexibility, is greatly pursued by chemists and material scientists.[41,42] Many graphene-based hybrids (such as LiV_3O_4@graphene,[33] Co_3O_4@graphene,[35] and MoO_2@graphene[36]), in which nanoparticles are distributed onto the surface of graphene or between graphene layers, have been fabricated by restacking graphene sheets in the presence of guest nanoparticles or corresponding precursors. However, as far as we know, monoclinic β-$Na_{0.33}V_2O_5$-graphene hybrids have not been reported yet.

Here, we successfully fabricated the $Na_{0.33}V_2O_5$ nanosheet-graphene hybrids for the first time. A two-step route involving a novel hydrothermal method and a freeze-drying technique was employed. First, we fabricated well-dispersed quasi-2D $Na_{0.33}V_2O_5$ nanosheets by a novel hydrothermal method using polyvinylpyrrolidone as the surfactant which benefited the formation of quasi-2D $Na_{0.33}V_2O_5$ nanosheets. Then the $Na_{0.33}V_2O_5$ nanosheets were inserted into graphene by freeze-drying. The $Na_{0.33}V_2O_5$ nanosheet-graphene hybrids have typical sandwich-like nanostructures. Graphene layers in the hybrids build a conducting network and prevent nanosheets from agglomerating during cycling, which can shorten the transport path for electrons and lithium ions.[43,44] It is surprising that the $Na_{0.33}V_2O_5$ nanosheet-graphene hybrids show superior rate performance even at extremely high current densities (up to 9 A·g^{-1}), which is much better than those reported $Na_{0.33}V_2O_5$ materials[9,16,17] and some vanadates containing other metal ions.[4−8] This strategy could be explored to obtain composites consisting of graphene and other ternary materials with complex valence states and nonlayered crystal structures.

EXPERIMENTAL SECTION

Materials Preparation. All of the raw materials were of analytical grade and used as received without any further purification.

$Na_{0.33}V_2O_5$ nanosheets were first prepared via a hydrothermal method. Vanadium pentoxide (V_2O_5, 0.364 g) was dissolved in 35 mL of a mixture of deionized water and 30 wt % hydrogen peroxide (6:1, v/v) with vigorous stirring. Then sodium bicarbonate ($NaHCO_3$, 0.126 g) and polyvinylpyrrolidone (PVP, 0.5 g) were added under magnetic stirring until a clear solution formed. The final mixture was transferred to a 50 mL Teflon-lined stainless steel autoclave and heated at 160 °C for 3 h to form the precursor of $Na_{0.33}V_2O_5$. Then the resulting precipitate was washed by centrifugation and dried at 70 °C overnight; after that it was calcined at 350 °C for 6 h in air to obtain $Na_{0.33}V_2O_5$ nanosheets. Graphene oxide (GO) was synthesized by Hummers' method.[45]

$Na_{0.33}V_2O_5$ nanosheet-graphene hybrids were fabricated by subsequent freeze-drying and thermal reduction. An 80 mg amount of the as-synthesized $Na_{0.33}V_2O_5$ was homogeneously dispersed in 30 mL of GO dispersion (1.5 mg/mL) using a probe sonication. The mixture was freeze-dried and formed sponge-like $Na_{0.33}V_2O_5$-graphene oxide hybrids which were then calcined at 280 °C for 1 h in air to obtain $Na_{0.33}V_2O_5$ and thermally reduced graphene hybrids.[46] Pure thermally reduced graphene was also prepared via the same processes

DOI: 10.1021/acsami.5b04827
ACS Appl. Mater. Interfaces 2015, 7, 17433−17440

of freeze-drying and thermal reduction as $Na_{0.33}V_2O_5$ nanosheet-graphene hybrids without adding $Na_{0.33}V_2O_5$ nanosheets.

The obtained thermally reduced graphene, $Na_{0.33}V_2O_5$, $Na_{0.33}V_2O_5$-graphene oxide, and $Na_{0.33}V_2O_5$-thermally reduced graphene are designated as TRG, NVO, NVO-GO, and NVO-TRG, respectively.

Materials Characterization. The structures and morphologies of as-prepared samples were characterized by X-ray diffraction (XRD; Rigaku D/max2500; Cu Kα radiation), scanning electron microscope (SEM; FEI Nova NanoSEM 230; 10 kV), transmission electron microscope (TEM; JEOL JEM-2100F; 200 kV), atomic force microscopy (AFM; Picoplus), and Raman spectroscopy (Jobin Yvon LabRAM Hr800, Longjumeau, France). The content of graphene in the NVO-TRG hybrids was measured by a combined differential scanning calorimetry (DSC) and thermogravimetric analysis (TGA) instrument (Netzsch STA449C, Selb, Germany) in an air atmosphere.

Electrochemical Measurements. Electrochemical tests were carried out via CR2016 coin-type cells. The working electrodes were fabricated by mixing the active material, acetylene black, and polyvinylidene fluoride (PVDF) in a weight ratio of 7:2:1 in an appropriate amount of *N*-methyl-2-pyrrolidone (NMP). The resulting slurry was then cast onto Al foil and dried in a vacuum oven at 100 °C for 10 h. Li metal, polyethylene membrane, and 1 M $LiPF_6$ solution in ethylene carbonate/dimethyl carbonate (EC/DMC; 1:1, v/v) were used as counter electrodes, separators, and the electrolyte, respectively. All coin cells were assembled in an argon-filled glovebox (Mbraun, Garching, Germany).

The galvanostatic charge/discharge measurements were conducted in the voltage range of 1.5−4.0 V (vs Li/Li^+) at room temperature using a battery tester (CT2001A, LANHE, Wuhan, China). The current densities and specific capacities were based on the weights of $Na_{0.33}V_2O_5$ nanosheets only. Cyclic voltammetry (CV) measurements were performed at a scan rate of 0.1 $mV{\cdot}s^{-1}$ in the voltage range of 1.5−4.0 V (vs Li/Li^+) on an electrochemical workstation (CHI604E, ChenHua, Shanghai, China). The electrochemical impendence spectrometry (EIS) tests were carried out in the frequency range of 100 kHz to 10 mHz on cells in as-assembled condition using an electrochemical workstation (ZAHNER-IM6ex, Kronach, Germany).

RESULTS AND DISCUSSION

The phases of as-synthesized samples were characterized by XRD, and the results are shown in Figure 2a. All three samples (NVO nanosheets, NVO-GO hybrids, and NVO-TRG hybrids) show similar diffraction peaks which could be well-indexed to a monoclinic β-$Na_{0.33}V_2O_5$ phase (JCPDS No. 77-0146). These results indicate that the crystal structures of NVO nanosheets in NVO-GO and NVO-TRG hybrids are well-preserved during the processes of freeze-drying and thermal reduction. In the pattern of TRG, the sharp diffraction peak of GO located at 10.6° vanishes but a new broad diffraction peak around 25° appears, indicating the deep reduction of GO.[46] Correspondingly, the broad (100) peak of NVO-GO hybrids which suggests the existence of GO is also narrowed in the pattern of NVO-TRG hybrids. However, the characteristic peak of TRG is indistinctive in the pattern of NVO-TRG hybrids, perhaps because it is shaded by the strong diffraction peaks of NVO nanosheets.[33] In the pattern of NVO nanosheets, the intensity of the (002) peak is slightly stronger than that of the $(11\bar{1})$ peak which is the strongest peak in the standard card of β-$Na_{0.33}V_2O_5$. This result implies the preferred orientation of NVO nanosheets along the (002) plane. However, for NVO-TRG hybrids, the (002) peak intensity of NVO nanosheets is far stronger than the $(11\bar{1})$ peak intensity, which might be attributed to the enhanced alignment of NVO nanosheets on large graphene layers.

Raman spectroscopy was used to characterize graphene layers in NVO-TRG hybrids (Figure 2b). The Raman spectra of

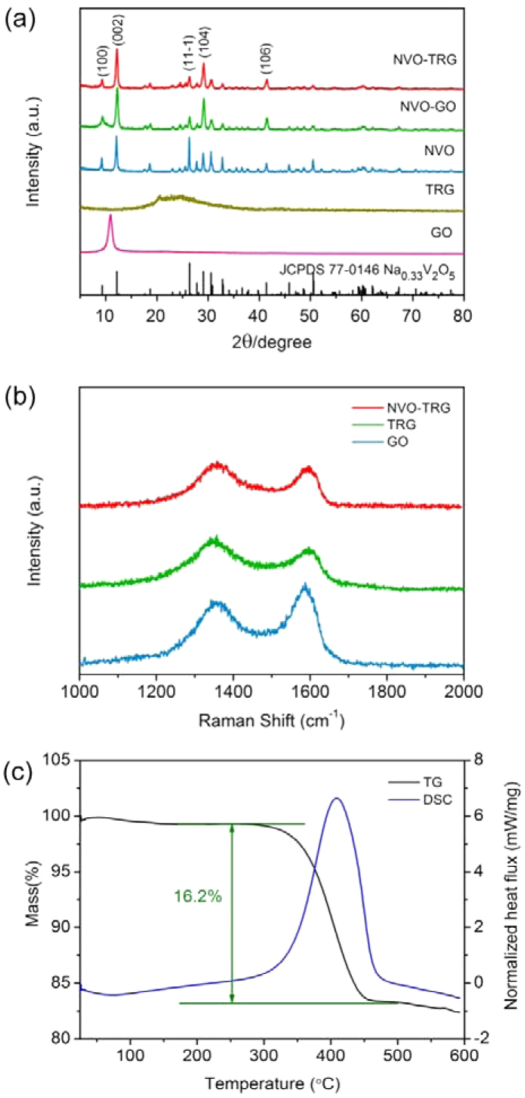

Figure 2. (a) XRD patterns of GO, TRG, NVO nanosheets, NVO-GO hybrids, and NVO-TRG hybrids. (b) Raman spectra of GO, TRG, and NVO-TRG hybrids. (c) TG and DSC curves of the as-prepared NVO-TRG hybrids.

all three samples show similar peaks at about 1356 and 1580 cm^{-1} which can be separately assigned to the symmetry A_{1g} mode (D band) and the E_{2g} mode of sp^2 carbon atoms (G band). It can be seen that the intensity ratios of D band to G band (I_D/I_G) of TRG and NVO-TRG (about 1.18 and 1.13) are higher than that of GO (about 0.81). The increasing I_D/I_G indicates the effectiveness of thermal reduction of GO, which is consistent with the XRD results.[47]

The TG result of NVO-TRG hybrids, as shown in Figure 2c, shows a mass loss of about 16.2%. And the corresponding DSC curve shows a clear exothermic peak around 400 °C, suggesting that the mass loss should be ascribed to the combustion of TRG. Accordingly, the content of TRG in the NVO-TRG hybrids can be deduced.

Figure 3a displays that the precursor of NVO consists of nanosheets with width of 200−300 nm and length of 0.5−1 μm. The nanosheet morphology is well-maintained after calcination as shown in Figure 3b. AFM testing gives a direct thickness of NVO nanosheets, which is about 30 nm, as shown in Figure S1 of the Supporting Information. The images of

DOI: 10.1021/acsami.5b04827
ACS Appl. Mater. Interfaces 2015, 7, 17433−17440

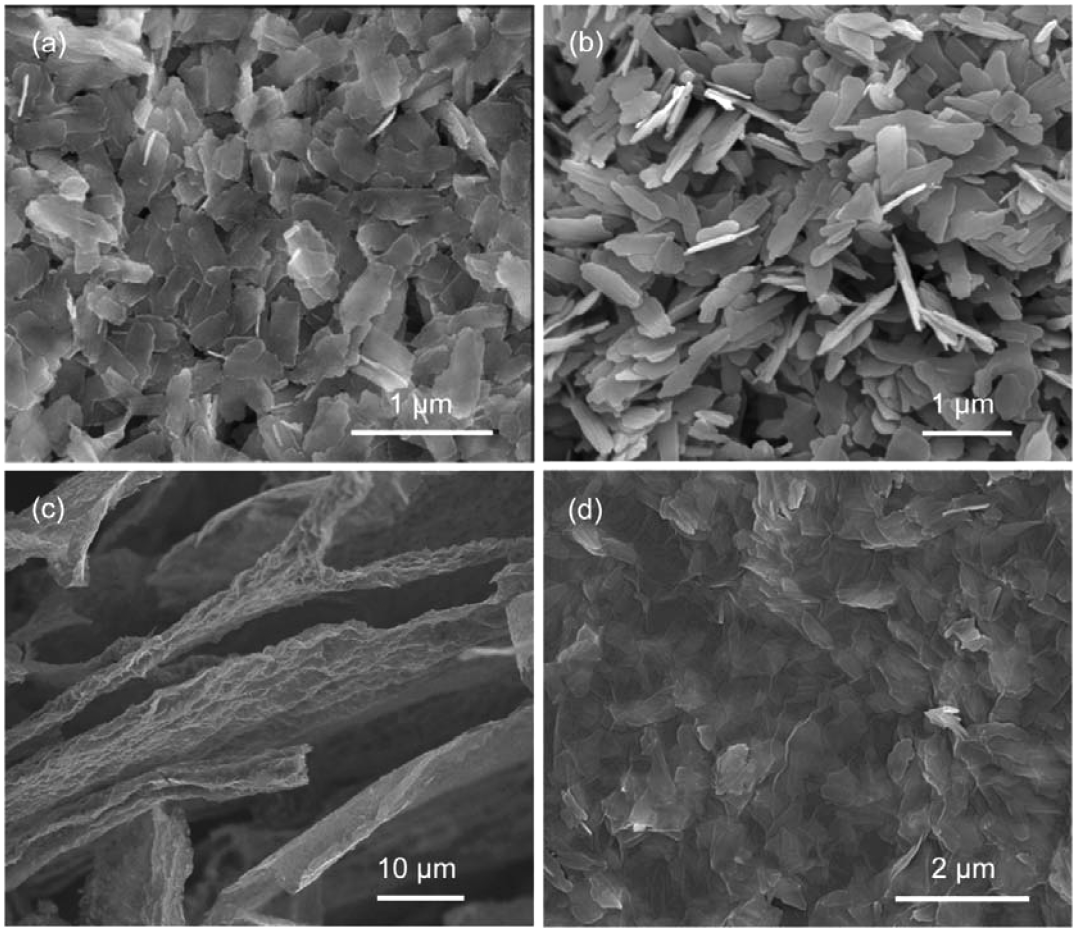

Figure 3. SEM images of (a) the precursor of NVO and (b) NVO nanosheets; (c) side view and (d) top view of NVO-TRG hybrids.

NVO-TRG hybrids show that dispersed NVO nanosheets are well-covered by wrinkled graphene layers and the NVO-TRG hybrids show a layer-by-layer structure (Figure 3c,d).

To provide further insights into the morphology and structure of the resulting NVO-TRG hybrids, TEM investigations were carried out. The bright-field TEM (BF TEM) image of NVO-TRG hybrids is shown in Figure 4a. And the

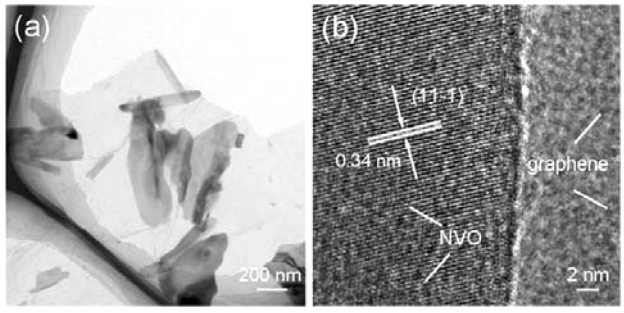

Figure 4. (a) BF TEM and (b) HRTEM images of NVO-TRG hybrids.

clear lattice fringes with a spacing of 0.34 nm in the high-resolution TEM (HRTEM) image can be indexed to the (11$\bar{1}$) plane of the monoclinic β-$Na_{0.33}V_2O_5$, which is consistent with the XRD results (Figure 4b). A detailed chemical analysis of NVO-TRG hybrids was conducted using high-angle annular dark-field (HAADF) scanning transmission electron microscopy (STEM) and energy dispersive X-ray (EDX) elemental mapping. Parts a and b of Figure S2 separately show the BF TEM and HAADF STEM images of the NVO-TRG hybrids. The elemental mappings of the constituting elements C, Na, V, and O (Figure S2c–f), which demonstrate the compositional distribution of the hybrids, show clear boundaries of NVO nanosheets and graphene.

The preceding XRD, Raman, SEM, and TEM results indicate that the NVO-TRG hybrids have sandwich-like nanostructures with NVO nanosheets well-dispersed between graphene layers. These unique nanostructures are expected for superior electrochemical performance because they can shorten the transport path for electrons and lithium ions.

The electrochemical properties of NVO-TRG hybrids and bare NVO nanosheets as cathode materials for lithium ion batteries were studied in detail. Figure 5a shows cyclic voltammetry (CV) curves of NVO-TRG electrode. The redox peaks of NVO-TRG electrode are located at about 3.26, 2.88, 2.50, and 1.97 V for the cathodic process and about 2.39, 2.77, 2.95, and 3.32 V for the anodic process. Those cathodic and anodic peaks can be ascribed to the multistep lithium ion intercalation and deintercalation behaviors in β-$Na_{0.33}V_2O_5$, respectively.[16,17,48] Besides, the shapes of the CV curves are almost identical, suggesting highly reversible lithium insertion and extraction processes in the NVO-TRG electrode. As for NVO electrode, the CV curves show similar redox peaks with cathodic peaks at around 3.26, 2.87, 2.45, and 1.91 V and anodic peaks at around 2.34, 2.83, 2.98, and 3.34 V, but these

DOI: 10.1021/acsami.5b04827
ACS Appl. Mater. Interfaces 2015, 7, 17433−17440

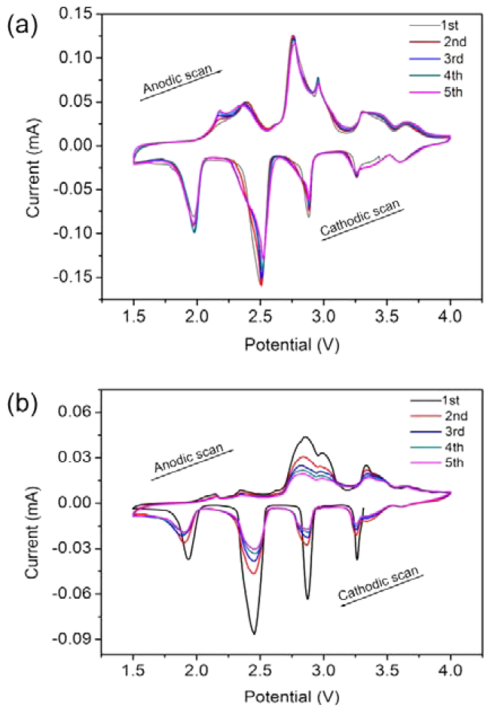

Figure 5. Cyclic voltammetry profiles of (a) NVO-TRG and (b) NVO electrodes.

redox peaks are less reversible than those of NVO-TRG electrode (Figure 5b).

Figure 6a displays the discharge (Li lithiation)/charge (Li delithiation) profiles of NVO-TRG electrode at a current density of 150 mA·g^{-1}. Discharge plateaus at about 3.25, 2.90, 2.54, and 2.03 V as well as charge plateaus at about 2.71, 2.95, and 3.29 V can be observed in the first cycle, which is consistent with the CV results. All of the profiles show similar multistep discharge/charge behaviors, which also indicates the highly reversible processes of lithium intercalation and deintercalation in the NVO-TRG electrode.

The cycling performance of NVO-TRG and NVO electrodes at different current densities are shown in Figure 6b. The NVO-TRG hybrids can maintain discharge capacities of 310 and 298 mA·h·g^{-1} at 150 and 300 mA·g^{-1} over 50 cycles, with high capacity retention of 94.8% and 94.9% on the basis of maximum discharge capacities. For the NVO electrode, the initial discharge capacities of 258 and 234 mA·h·g^{-1} are delivered at the current densities of 150 and 300 mA·g^{-1}. However, the discharge capacities of NVO electrode decrease rapidly during the first few cycles, with low-capacity retentions of 70.2% and 55.6% at 150 and 300 mA·g^{-1} over 50 cycles.

More surprising results come from further studies of the rate capability of NVO-TRG electrode. Figure 6c shows the rate performance of NVO-TRG and NVO electrodes tested at different current densities. NVO-TRG electrode exhibits discharge capacities of 313, 276, 232, and 191 mA·h·g^{-1} during the 10th cycle at the current densities of 0.3, 1.5, 3, and 4.5 A·g^{-1}, respectively. Notably, even at extremely high current densities of 6.0, 7.5, and 9.0 A·g^{-1}, NVO-TRG electrode can still deliver desirable capacities of 159, 130, and 108 mA·h·g^{-1}. Moreover, NVO-TRG electrode also exhibits an excellent cycling stability at a high current density of 4.5 A·g^{-1} as shown in Figure 6d, maintaining a discharge capacity of 199 mA·h·g^{-1} after 400 cycles. Interestingly, the cycling profile exhibits an obviously increasing trend in the initial stage. In some previous works on vanadates, a similar capacity increase was also observed.[9,17] This phenomenon might be attributed to the

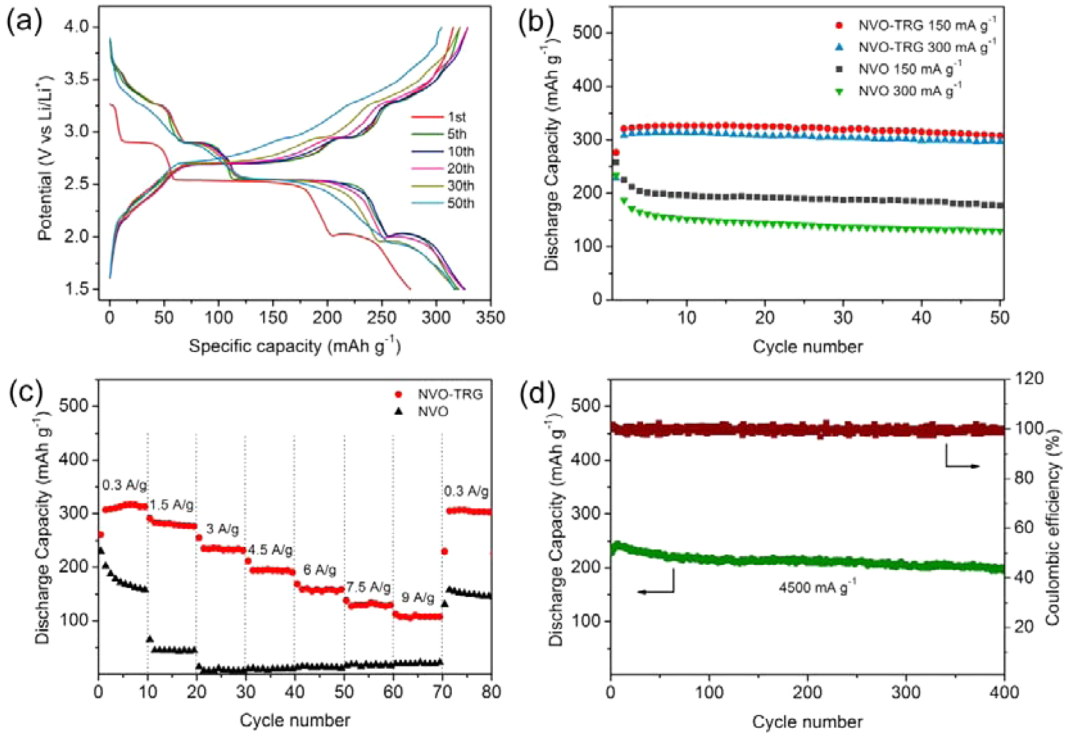

Figure 6. (a) Discharge and charge profiles of NVO-TRG electrode at a current of 150 mA·g^{-1} in the range of 1.5−4 V vs Li/Li$^+$. (b) Cycling performance of NVO-TRG and NVO electrodes at different current densities. (c) Rate performance of NVO-TRG and NVO electrodes. (d) Cycling performance of NVO-TRG electrode at a current density of 4500 mA·g^{-1} and the corresponding efficiency.

DOI: 10.1021/acsami.5b04827
ACS Appl. Mater. Interfaces 2015, 7, 17433−17440

Table 1. Comparison on Electrochemical Properties of $Na_{0.33}V_2O_5$-Graphene Hybrids and Other Works in Coin Cell Configuration

sample	ref	current density ($mA·g^{-1}$)	capacity after cycles ($mA·h·g^{-1}$)	cycle no. (capacity retension)	voltage range (V)
$Li_{0.7}V_6O_{15}$ nanowire	8	1000	~50	900 (39%)	1.5−4.0
Mo-doped LiV_3O_8	6	300	205.9	100 (76.5%)	2.0−4.0
Al_2O_3-coated LiV_3O_8	4	100	205.7	100 (72.7%)	2.0−4.0
		3000	118.5	100 (74.0%)	2.0−4.0
LiV_3O_8 nanowire	7	1500	160	400 (90.9%)	1.5−4.0
		2000	120	600 (87.6%)	1.5−4.0
3D $AgVO_3$/graphene composite aerogels	5	50	118.8	50 (60.9%)	1.5−3.7
		1000	116.4	50 (80.9%)	1.5−3.7
mesoporous β-$Na_{0.33}V_2O_5$	16	50	177	50 (60.2%)	1.5−4.0
		300	154	50 (61.0%)	1.5−4.0
NaV_6O_{15} nanorods	9	20	328	20	1.5−4.5
		50	297	70	1.5−4.5
β-$Na_{0.33}V_2O_5$	17	3.8	253	70 (89%)	1.5−4.0
$Na_{0.33}V_2O_5$-graphene hybrids	this work	150	310	50 (94.8%)	1.5−4.0
		300	298	50 (94.9%)	1.5−4.0
		4500	199	400 (87.4%)	1.5−4.0

process of activation and stabilization in the electrode materials.[11,49,50] In comparison, NVO electrode suffers from low discharge capacities, once the current densities reach 1.5 $A·g^{-1}$. The preceding results demonstrate that the electrochemical performance (especially the rate capability) of NVO-TRG hybrids is superior to that of NVO nanosheets. It is generally assumed that the charge/discharge rate capability of LIBS depends critically on the migration rate of lithium ions and electrons.[51−53] Therefore, the superior rate performance of NVO-TRG hybrids might be ascribed to its special sandwich-like nanostructures in which the combination of NVO nanosheets and graphene layers can benefit the transport of lithium ions and electrons. Table 1 gives a direct comparison on electrochemical properties of $Na_{0.33}V_2O_5$-graphene hybrids and other works. It can be seen that the $Na_{0.33}V_2O_5$-graphene hybrids show outstanding electrochemical performance.

To further understand the improved electrochemical performance of NVO-TRG electrode, electrochemical impedance spectroscopy measurements of fresh NVO-TRG and NVO electrodes were performed as shown in Figure 7. Both Nyquist plots show a compressed semicircle in the high- to medium-frequency range and an inclined line in the low-frequency range. In general, the semicircle describes the charge transfer resistance, and the line is related to the diffusion of lithium ions within the electrode. The impedance spectra can well-fit into the equivalent circuit shown in the inset of Figure 7, where the symbols R_s, R_{ct}, CPE_{dl}, and Z_w stand for the solution resistance, charge transfer resistance, double layer capacitance, and Warburg impedance, respectively. The charge transfer resistance of NVO-TRG electrode (158 Ω) is much smaller than that of NVO electrode (588 Ω). This is clear evidence that NVO-TRG electrode has a higher electronic conductivity than NVO electrode. Thus, the improved electrochemical performance of NVO-TRG electrode could be attributed to the presence of graphene layers. Graphene layers can act as miniature current collectors and separators between NVO nanosheets to establish a conducting network and prevent NVO nanosheets from agglomerating during cycling, which facilitates fast electron and ion transport in the electrode.

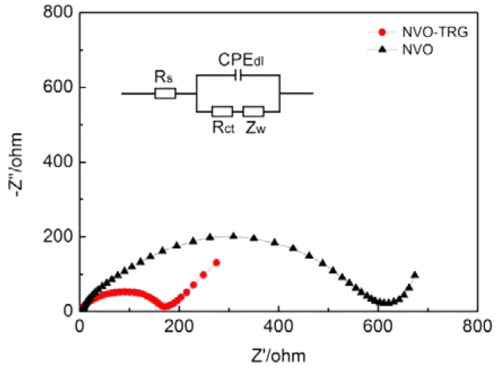

Figure 7. Nyquist plots of the NVO-TRG and NVO electrodes.

CONCLUSIONS

$Na_{0.33}V_2O_5$ nanosheet-graphene hybrids were successfully fabricated for the first time. The strategy mainly involves a novel hydrothermal method and a freeze-drying technique. It is interesting that the $Na_{0.33}V_2O_5$-graphene hybrids demonstrate highly reversible capacity, good cycling stability, and superior rate performance compared with those reported $Na_{0.33}V_2O_5$ materials and some vanadates containing other metal ions. A desirable reversible capacity of 310 $mA·h·g^{-1}$ can be delivered at a current density of 150 $mA·g^{-1}$, with high-capacity retention of 94.8% after 50 cycles. Moreover, the $Na_{0.33}V_2O_5$-graphene hybrids can maintain a discharge capacity of 199 $mA·h·g^{-1}$ after 400 cycles even at an extremely high current density of 4.5 $A·g^{-1}$, with an average fading rate of 0.03% per cycle. Considering their surprising rate performance, the $Na_{0.33}V_2O_5$-graphene hybrids could be a promising candidate for high-power lithium ion batteries.

ASSOCIATED CONTENT

Supporting Information

The Supporting Information is available free of charge on the ACS Publications website at DOI: 10.1021/acsami.5b04827.

AFM image of NVO nanosheets, BF TEM and HAADF STEM images of NVO-TRG hybrids, and corresponding EDX mapping images of NVO-TRG hybrids (PDF).

DOI: 10.1021/acsami.5b04827
ACS Appl. Mater. Interfaces 2015, 7, 17433−17440

AUTHOR INFORMATION

Corresponding Author

*E-mail: liujun4982004@csu.edu.cn.

Notes

The authors declare no competing financial interest.

ACKNOWLEDGMENTS

This work is supported by the National Natural Science Foundation of China (Grant Nos. 51202297, 51472271, 61376018, and 51174233), the Program for New Century Excellent Talents in University (Grant NCET-12-0554), and the 2011 Program.

REFERENCES

(1) Armand, M.; Tarascon, J.-M. Building Better Batteries. *Nature* **2008**, *451*, 652−657.

(2) Fergus, J. W. Recent Developments in Cathode Materials for Lithium Ion Batteries. *J. Power Sources* **2010**, *195*, 939−954.

(3) Wang, Y.; Takahashi, K.; Lee, K.; Cao, G. Nanostructured Vanadium Oxide Electrodes for Enhanced Lithium-Ion Intercalation. *Adv. Funct. Mater.* **2006**, *16*, 1133−1144.

(4) Huang, S.; Tu, J.; Jian, X.; Lu, Y.; Shi, S.; Zhao, X.; Wang, T.; Wang, X.; Gu, C. Enhanced Electrochemical Properties of Al_2O_3-Coated LiV_3O_8 Cathode Materials for High-Power Lithium-Ion Batteries. *J. Power Sources* **2014**, *245*, 698−705.

(5) Liang, L.; Xu, Y.; Lei, Y.; Liu, H. 1-Dimensional $AgVO_3$ Nanowires Hybrid with 2-Dimensional Graphene Nanosheets to Create 3-Dimensional Composite Aerogels and Their Improved Electrochemical Properties. *Nanoscale* **2014**, *6*, 3536−3539.

(6) Song, H.; Liu, Y.; Zhang, C.; Liu, C.; Cao, G. Mo-Doped LiV_3O_8 Nanorod-Assembled Nanosheets as a High Performance Cathode Material for Lithium Ion Batteries. *J. Mater. Chem. A* **2015**, *3*, 3547−3558.

(7) Xu, X.; Luo, Y.-Z.; Mai, L.-Q.; Zhao, Y.-L.; An, Q.-Y.; Xu, L.; Hu, F.; Zhang, L.; Zhang, Q.-J. Topotactically Synthesized Ultralong LiV_3O_8 Nanowire Cathode Materials for High-Rate and Long-Life Rechargeable Lithium Batteries. *NPG Asia Mater.* **2012**, *4*, e20.

(8) Zhao, Y.; Han, C.; Yang, J.; Su, J.; Xu, X.; Li, S.; Xu, L.; Fang, R.; Jiang, H.; Zou, X.; et al. Stable Alkali Metal Ion Intercalation Compounds as Optimized Metal Oxide Nanowire Cathodes for Lithium Batteries. *Nano Lett.* **2015**, *15*, 2180−2185.

(9) Liu, H. M.; Wang, Y. G.; Li, L.; Wang, K. X.; Hosono, E.; Zhou, H. S. Facile Synthesis of NaV_6O_{15} Nanorods and Its Electrochemical Behavior as Cathode Material in Rechargeable Lithium Batteries. *J. Mater. Chem.* **2009**, *19*, 7885−7891.

(10) Wang, H.; Liu, S.; Ren, Y.; Wang, W.; Tang, A. Ultrathin $Na_{1.08}V_3O_8$ Nanosheets-a Novel Cathode Material with Superior Rate Capability and Cycling Stability for Li-Ion Batteries. *Energy Environ. Sci.* **2012**, *5*, 6173−6179.

(11) Liang, S.; Chen, T.; Pan, A.; Liu, D.; Zhu, Q.; Cao, G. Synthesis of $Na_{1.25}V_3O_8$ Nanobelts with Excellent Long-Term Stability for Rechargeable Lithium-Ion Batteries. *ACS Appl. Mater. Interfaces* **2013**, *5*, 11913−11917.

(12) Owens, B. B.; Passerini, S.; Smyrl, W. H. Lithium Ion Insertion in Porous Metal Oxides. *Electrochim. Acta* **1999**, *45*, 215−224.

(13) Muster, J.; Kim, G. T.; Krstić, V.; Park, J. G.; Park, Y. W.; Roth, S.; Burghard, M. Electrical Transport through Individual Vanadium Pentoxide Nanowires. *Adv. Mater.* **2000**, *12*, 420−424.

(14) Xu, Y.; Han, X.; Zheng, L.; Yan, W.; Xie, Y. Pillar Effect on Cyclability Enhancement for Aqueous Lithium Ion Batteries: A New Material of β-Vanadium Bronze $M_{0.33}V_2O_5$ (M = Ag, Na) Nanowires. *J. Mater. Chem.* **2011**, *21*, 14466−14472.

(15) Baddour-Hadjean, R.; Bach, S.; Emery, N.; Pereira-Ramos, J. P. The Peculiar Structural Behaviour of β-$Na_{0.33}V_2O_5$ Upon Electrochemical Lithium Insertion. *J. Mater. Chem.* **2011**, *21*, 11296−11305.

(16) Liang, S.; Zhou, J.; Fang, G.; Zhang, C.; Wu, J.; Tang, Y.; Pan, A. Synthesis of Mesoporous β-$Na_{0.33}V_2O_5$ with Enhanced Electrochemical Performance for Lithium Ion Batteries. *Electrochim. Acta* **2014**, *130*, 119−126.

(17) Kim, J.-K.; Senthilkumar, B.; Sahgong, S. H.; Kim, J.-H.; Chi, M.; Kim, Y. New Chemical Route for the Synthesis of β-$Na_{0.33}V_2O_5$ and Its Fully Reversible Li Intercalation. *ACS Appl. Mater. Interfaces* **2015**, *7*, 7025−7032.

(18) Yamada, H.; Ueda, Y. Magnetic, Electric and Structural Properties of β-$A_xV_2O_5$ (A = Na, Ag). *J. Phys. Soc. Jpn.* **1999**, *68*, 2735−2740.

(19) Zhu, J.; Yin, Z.; Li, H.; Tan, H.; Chow, C. L.; Zhang, H.; Hng, H. H.; Ma, J.; Yan, Q. Bottom-up Preparation of Porous Metal-Oxide Ultrathin Sheets with Adjustable Composition/Phases and Their Applications. *Small* **2011**, *7*, 3458−3464.

(20) Choi, M.; Na, K.; Kim, J.; Sakamoto, Y.; Terasaki, O.; Ryoo, R. Stable Single-Unit-Cell Nanosheets of Zeolite Mfi as Active and Long-Lived Catalysts. *Nature* **2009**, *461*, 246−249.

(21) Rui, X.; Lu, Z.; Yu, H.; Yang, D.; Hng, H. H.; Lim, T. M.; Yan, Q. Ultrathin V_2O_5 Nanosheet Cathodes: Realizing Ultrafast Reversible Lithium Storage. *Nanoscale* **2013**, *5*, 556−560.

(22) Xu, C.; Zeng, Y.; Rui, X.; Xiao, N.; Zhu, J.; Zhang, W.; Chen, J.; Liu, W.; Tan, H.; Hng, H. H.; Yan, Q. Controlled Soft-Template Synthesis of Ultrathin C@Fes Nanosheets with High-Li-Storage Performance. *ACS Nano* **2012**, *6*, 4713−4721.

(23) Liu, J.; Liu, X.-W. Two-Dimensional Nanoarchitectures for Lithium Storage. *Adv. Mater.* **2012**, *24*, 4097−4111.

(24) Zhang, B.; Han, Y.-d.; Zheng, J.-c.; Zhang, J.-f.; Shen, C.; Ming, L.; Yuan, X.-b.; Li, H. $VOPO_4$ Nanosheets as Anode Materials for Lithium-Ion Batteries. *Chem. Commun.* **2014**, *50*, 11132−11134.

(25) Zheng, J.-c.; Han, Y.-d.; Zhang, B.; Shen, C.; Ming, L.; Ou, X.; Zhang, J.-f. Electrochemical Properties of VPO_4/C Nanosheets and Microspheres as Anode Materials for Lithium-Ion Batteries. *ACS Appl. Mater. Interfaces* **2014**, *6*, 6223−6226.

(26) Rui, X.; Lu, Z.; Yin, Z.; Sim, D. H.; Xiao, N.; Lim, T. M.; Hng, H. H.; Zhang, H.; Yan, Q. Oriented Molecular Attachments through Sol-Gel Chemistry for Synthesis of Ultrathin Hydrated Vanadium Pentoxide Nanosheets and Their Applications. *Small* **2013**, *9*, 716−721.

(27) Wang, X.; Zhi, C.; Li, L.; Zeng, H.; Li, C.; Mitome, M.; Golberg, D.; Bando, Y. Chemical Blowing" of Thin-Walled Bubbles: High-Throughput Fabrication of Large-Area, Few-Layered BN and C_x-BN Nanosheets. *Adv. Mater.* **2011**, *23*, 4072−4076.

(28) Zhou, W.; Yin, Z.; Du, Y.; Huang, X.; Zeng, Z.; Fan, Z.; Liu, H.; Wang, J.; Zhang, H. Synthesis of Few-Layer MoS_2 Nanosheet-Coated TiO_2 Nanobelt Heterostructures for Enhanced Photocatalytic Activities. *Small* **2013**, *9*, 140−147.

(29) Huang, Y.; Li, Y.; Hu, Z.; Wei, G.; Guo, J.; Liu, J. A Carbon Modified MnO_2 Nanosheet Array as a Stable High-Capacitance Supercapacitor Electrode. *J. Mater. Chem. A* **2013**, *1*, 9809−9813.

(30) Jiang, H.; Zhao, T.; Li, C.; Ma, J. Hierarchical Self-Assembly of Ultrathin Nickel Hydroxide Nanoflakes for High-Performance Supercapacitors. *J. Mater. Chem.* **2011**, *21*, 3818−3823.

(31) Ma, R.; Takada, K.; Fukuda, K.; Iyi, N.; Bando, Y.; Sasaki, T. Topochemical Synthesis of Monometallic (Co^{2+}-Co^{3+}) Layered Double Hydroxide and Its Exfoliation into Positively Charged $Co(OH)_2$ Nanosheets. *Angew. Chem., Int. Ed.* **2008**, *47*, 86−89.

(32) Tang, Y. F.; Yang, L.; Qiu, Z.; Huang, J. S. Preparation and Electrochemical Lithium Storage of Flower-Like Spinel $Li_4Ti_5O_{12}$ Consisting of Nanosheets. *Electrochem. Commun.* **2008**, *10*, 1513−1516.

(33) Liu, J.; Lu, P.-J.; Liang, S.; Liu, J.; Wang, W.; Lei, M.; Tang, S.; Yang, Q. Ultrathin Li_3VO_4 Nanoribbon/Graphene Sandwich-Like Nanostructures with Ultrahigh Lithium Ion Storage Properties. *Nano Energy* **2015**, *12*, 709−724.

(34) Wang, H.; Cui, L.-F.; Yang, Y.; Sanchez Casalongue, H.; Robinson, J. T.; Liang, Y.; Cui, Y.; Dai, H. Mn_3O_4-Graphene Hybrid as a High-Capacity Anode Material for Lithium Ion Batteries. *J. Am. Chem. Soc.* **2010**, *132*, 13978−13980.

(35) Wu, Z.-S.; Ren, W.; Wen, L.; Gao, L.; Zhao, J.; Chen, Z.; Zhou, G.; Li, F.; Cheng, H.-M. Graphene Anchored with Co_3O_4 Nano-

DOI: 10.1021/acsami.5b04827
ACS Appl. Mater. Interfaces 2015, 7, 17433−17440

particles as Anode of Lithium Ion Batteries with Enhanced Reversible Capacity and Cyclic Performance. *ACS Nano* **2010**, *4*, 3187−3194.
(36) Yang, Q.; Liang, Q.; Liu, J.; Liang, S.; Tang, S.; Lu, P.; Lu, Y. Ultrafine MoO_2 Nanoparticles Grown on Graphene Sheets as Anode Materials for Lithium-Ion Batteries. *Mater. Lett.* **2014**, *127*, 32−35.
(37) Lu, P.-J.; Lei, M.; Liu, J. Graphene Nanosheets Encapsulated α-MoO_3 Nanoribbons with Ultrahigh Lithium Ion Storage Properties. *CrystEngComm* **2014**, *16*, 6745−6755.
(38) Qin, M.; Liu, J.; Liang, S.; Zhang, Q.; Li, X.; Liu, Y.; Lin, M. Facile Synthesis of Multiwalled Carbon Nanotube-V_2O_5 Nanocomposites as Cathode Materials for Li-Ion Batteries. *J. Solid State Electrochem.* **2014**, *18*, 2841−2846.
(39) Reddy, A. L. M.; Shaijumon, M. M.; Gowda, S. R.; Ajayan, P. M. Coaxial MnO_2/Carbon Nanotube Array Electrodes for High-Performance Lithium Batteries. *Nano Lett.* **2009**, *9*, 1002−1006.
(40) Yang, L.; Li, H.; Liu, J.; Sun, Z.; Tang, S.; Lei, M. Dual Yolk-Shell Structure of Carbon and Silica-Coated Silicon for High-Performance Lithium-Ion Batteries. *Sci. Rep.* **2015**, *5*, 10908.
(41) Sun, Y.; Wang, J.; Zhao, B.; Cai, R.; Ran, R.; Shao, Z. Binder-Free α-MoO_3 Nanobelt Electrode for Lithium-Ion Batteries Utilizing Van Der Waals Forces for Film Formation and Connection with Current Collector. *J. Mater. Chem. A* **2013**, *1*, 4736−4746.
(42) Dong, Y.; Li, S.; Xu, H.; Yan, M.; Xu, X.; Tian, X.; Liu, Q.; Mai, L. Wrinkled-Graphene Enriched MoO_3 Nanobelts with Increased Conductivity and Reduced Stress for Enhanced Electrochemical Performance. *Phys. Chem. Chem. Phys.* **2013**, *15*, 17165−17170.
(43) Lee, J. W.; Lim, S. Y.; Jeong, H. M.; Hwang, T. H.; Kang, J. K.; Choi, J. W. Extremely Stable Cycling of Ultra-Thin V_2O_5 Nanowire-Graphene Electrodes for Lithium Rechargeable Battery Cathodes. *Energy Environ. Sci.* **2012**, *5*, 9889−9894.
(44) Shen, L.; Yuan, C.; Luo, H.; Zhang, X.; Yang, S.; Lu, X. In Situ Synthesis of High-Loading $Li_4Ti_5O_{12}$-Graphene Hybrid Nanostructures for High Rate Lithium Ion Batteries. *Nanoscale* **2011**, *3*, 572−574.
(45) Hummers, W. S.; Offeman, R. E. Preparation of Graphitic Oxide. *J. Am. Chem. Soc.* **1958**, *80*, 1339−1339.
(46) Wang, Z.-l.; Xu, D.; Huang, Y.; Wu, Z.; Wang, L.-m.; Zhang, X.-b. Facile, Mild and Fast Thermal-Decomposition Reduction of Graphene Oxide in Air and Its Application in High-Performance Lithium Batteries. *Chem. Commun.* **2012**, *48*, 976−978.
(47) Stankovich, S.; Dikin, D. A.; Piner, R. D.; Kohlhaas, K. A.; Kleinhammes, A.; Jia, Y.; Wu, Y.; Nguyen, S. T.; Ruoff, R. S. Synthesis of Graphene-Based Nanosheets Via Chemical Reduction of Exfoliated Graphite Oxide. *Carbon* **2007**, *45*, 1558−1565.
(48) Bach, S.; Pereira-Ramos, J.; Baffier, N.; Messina, R. A Thermodynamic and Kinetic Study of Electrochemical Lithium Intercalation in $Na_{0.33}V_2O_5$ Bronze Prepared by a Sol-Gel Process. *J. Electrochem. Soc.* **1990**, *137*, 1042−1048.
(49) Qie, L.; Chen, W. M.; Wang, Z. H.; Shao, Q. G.; Li, X.; Yuan, L. X.; Hu, X. L.; Zhang, W. X.; Huang, Y. H. Nitrogen-Doped Porous Carbon Nanofiber Webs as Anodes for Lithium Ion Batteries with a Superhigh Capacity and Rate Capability. *Adv. Mater.* **2012**, *24*, 2047−2050.
(50) Wang, Z.; Chen, J. S.; Zhu, T.; Madhavi, S.; Lou, X. W. One-Pot Synthesis of Uniform Carbon-Coated MoO2 Nanospheres for High-Rate Reversible Lithium Storage. *Chem. Commun.* **2010**, *46*, 6906−6908.
(51) Li, N.; Chen, Z.; Ren, W.; Li, F.; Cheng, H.-M. Flexible Graphene-Based Lithium Ion Batteries with Ultrafast Charge and Discharge Rates. *Proc. Natl. Acad. Sci. U. S. A.* **2012**, *109*, 17360−17365.
(52) Liu, J.; Tang, S.; Lu, Y.; Cai, G.; Liang, S.; Wang, W.; Chen, X. Synthesis of Mo_2N Nanolayer Coated MoO_2 Hollow Nanostructures as High-Performance Anode Materials for Lithium-Ion Batteries. *Energy Environ. Sci.* **2013**, *6*, 2691−2697.
(53) Shen, L.; Yuan, C.; Luo, H.; Zhang, X.; Yang, S.; Lu, X. In Situ Synthesis of High-Loading $Li_4Ti_5O_{12}$-Graphene Hybrid Nanostructures for High Rate Lithium Ion Batteries. *Nanoscale* **2011**, *3*, 572−574.

DOI: 10.1021/acsami.5b04827
ACS Appl. Mater. Interfaces 2015, 7, 17433−17440